

RECEIVED BY TIC JUL 17 1979  
NUREG/CR-0900

# EVALUATION OF MATERIALS FOR RETENTION OF SODIUM AND CORE DEBRIS IN REACTOR SYSTEMS

MASTER

Annual Progress Report  
September 1977 - December 1978

D. G. Swanson  
E. H. Zehms                      R. A. Meyer  
J. D. McClelland                H. L. L. van Paassen

The Aerospace Corporation

Prepared for  
U. S. Nuclear Regulatory Commission

DISTRIBUTION OF THIS DOCUMENT IS UNLIMITED

## **DISCLAIMER**

**This report was prepared as an account of work sponsored by an agency of the United States Government. Neither the United States Government nor any agency Thereof, nor any of their employees, makes any warranty, express or implied, or assumes any legal liability or responsibility for the accuracy, completeness, or usefulness of any information, apparatus, product, or process disclosed, or represents that its use would not infringe privately owned rights. Reference herein to any specific commercial product, process, or service by trade name, trademark, manufacturer, or otherwise does not necessarily constitute or imply its endorsement, recommendation, or favoring by the United States Government or any agency thereof. The views and opinions of authors expressed herein do not necessarily state or reflect those of the United States Government or any agency thereof.**

## **DISCLAIMER**

**Portions of this document may be illegible in electronic image products. Images are produced from the best available original document.**

#### NOTICE

This report was prepared as an account of work sponsored by an agency of the United States Government. Neither the United States Government nor any agency thereof, or any of their employees, makes any warranty, expressed or implied, or assumes any legal liability or responsibility for any third party's use, or the results of such use, of any information, apparatus product or process disclosed in this report, or represents that its use by such third party would not infringe privately owned rights.

Available from  
National Technical Information Service  
Springfield, Virginia 22161

NUREG/CR-0900  
Aerospace Report No.  
ATR-79(7814)-1

ANNUAL PROGRESS REPORT  
EVALUATION OF MATERIALS FOR RETENTION OF  
SODIUM AND CORE DEBRIS IN REACTOR SYSTEMS

Prepared by D. G. Swanson, E. H. Zehms, R. A. Meyer,  
J. D. McClelland, and H. L. L. van Paassen  
Materials Sciences Laboratory

December 1978

Laboratory Operations  
THE AEROSPACE CORPORATION  
El Segundo, California 90245

Prepared for  
OFFICE OF NUCLEAR REACTOR REGULATION  
DIVISION OF PROJECT MANAGEMENT  
U. S. NUCLEAR REGULATORY COMMISSION  
Washington, D. C. 20555


Contract No. NRC-03-79-126

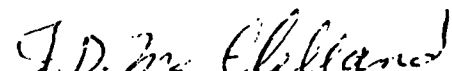
**DISTRIBUTION OF THIS DOCUMENT IS UNLIMITED**  
W.D.M.



ANNUAL PROGRESS REPORT  
EVALUATION OF MATERIALS FOR RETENTION OF  
SODIUM AND CORE DEBRIS IN REACTOR SYSTEMS

Prepared

  
\_\_\_\_\_  
D. G. Swanson

  
\_\_\_\_\_  
J. D. McClelland, Associate  
Director  
Materials Sciences Laboratory

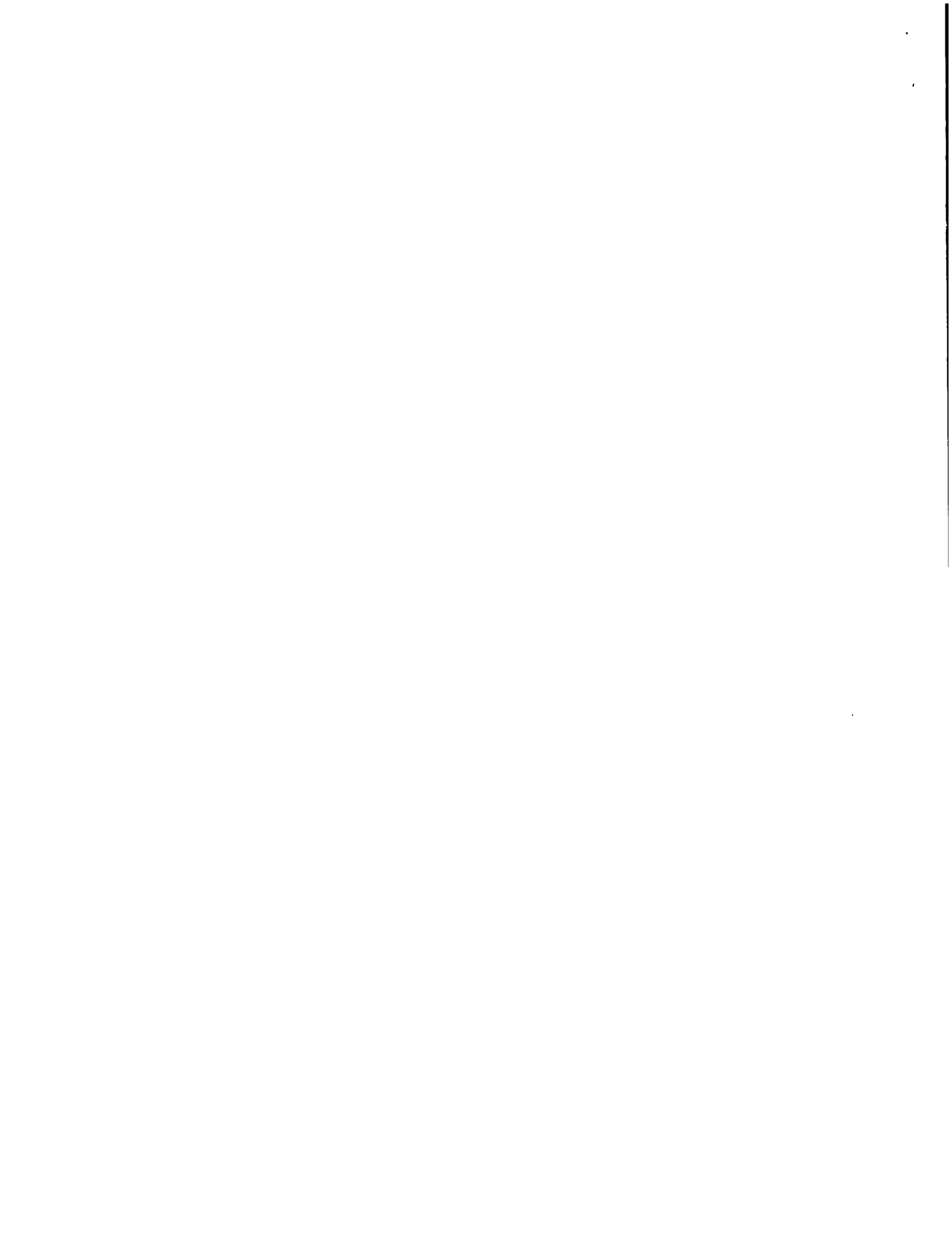
  
\_\_\_\_\_  
E. H. Zehms

  
\_\_\_\_\_  
H. L. L. van Paassen

  
\_\_\_\_\_  
R. A. Meyer, Head  
Carbon and Polymers Department

Approved

  
\_\_\_\_\_  
W. C. Riley, Director  
Materials Sciences Laboratory





## ABSTRACT

This report considers some of the consequences of a hypothetical core disruptive accident in a nuclear reactor. The interactions expected between molten core debris, liquid sodium, and materials that might be employed in an ex-vessel sacrificial-bed or in the reactor building are discussed. Experimental work performed for NRC by Sandia Laboratories and Hanford Engineering Development Laboratory on the interactions between liquid sodium and basalt concrete is reviewed. Studies of molten steel interactions with concrete at Sandia Laboratories and molten  $UO_2$  interactions with concrete at The Aerospace Corporation are also discussed. The potential of MgO for use in core containment is discussed and refractory materials other than MgO are reviewed. Finally, results from earlier experiments with molten core debris and various materials performed at The Aerospace Corporation are presented.



## CONTENTS

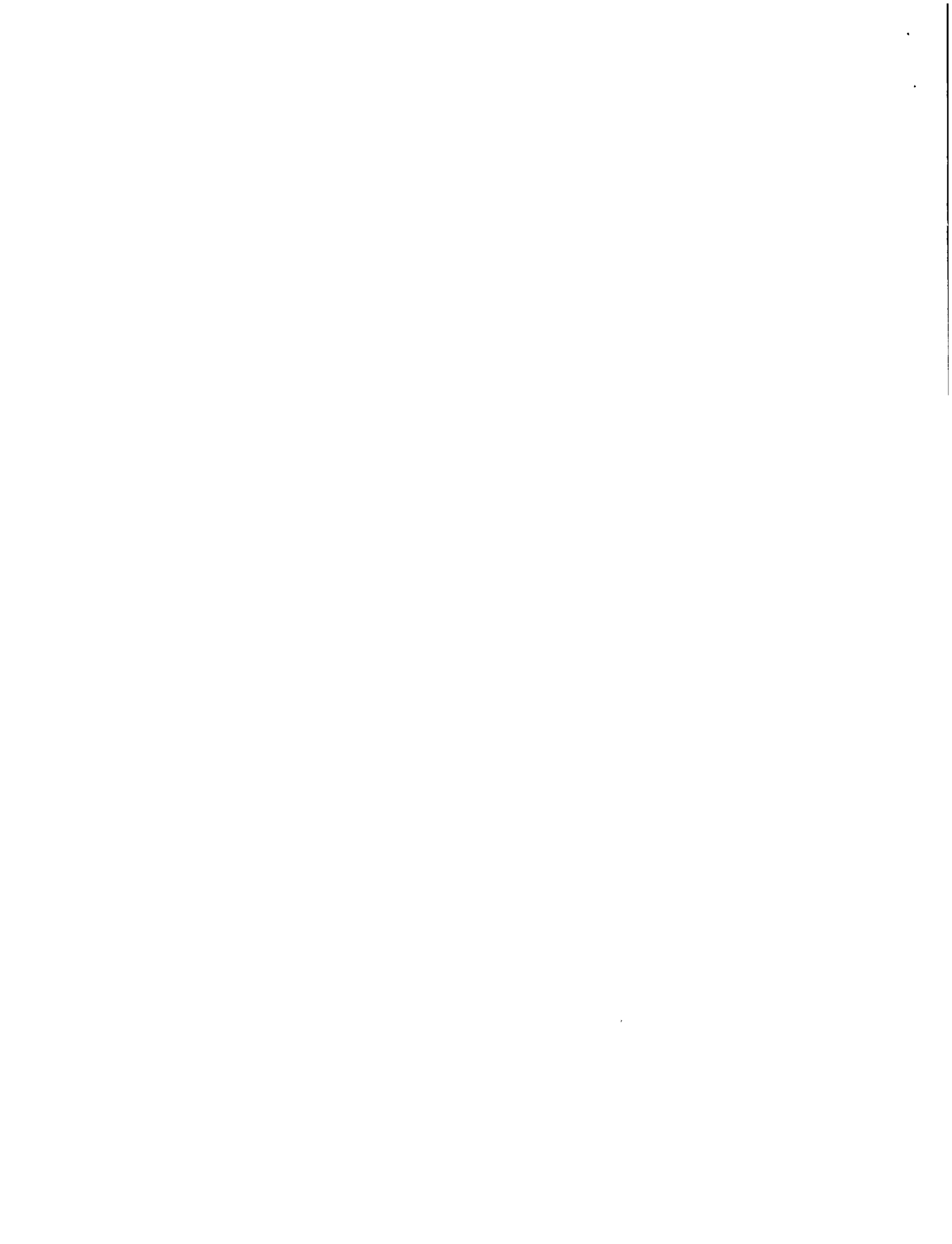
ABSTRACT . . . . .	v
I. INTRODUCTION . . . . .	1
II. SUMMARY . . . . .	3
A. Liquid Sodium-Basalt Concrete Interactions . . . . .	3
B. Molten Core Debris - Concrete Interactions . . . . .	3
C. Sacrificial Materials . . . . .	4
D. Refractory Materials Used in the FFTF . . . . .	4
E. Analysis of Specimens from Earlier Molten Core Debris-Concrete Experiments at The Aerospace Corporation . . . . .	5
III. LIQUID SODIUM - BASALT CONCRETE INTERACTIONS . . . . .	6
IV. MOLTEN CORE DEBRIS-CONCRETE INTERACTIONS . . . . .	11
A. Molten $UO_2$ . . . . .	11
B. Molten Steel Experiments . . . . .	12
C. Gas Generation . . . . .	14
D. Fission Product Distribution . . . . .	15
E. Scaling Considerations . . . . .	16
V. SACRIFICIAL MATERIALS . . . . .	17
A. Desirable Properties . . . . .	17
B. Available Materials . . . . .	18
C. Magnesium Oxide . . . . .	20
D. Mortars for Use With MgO . . . . .	23
E. Erosion of MgO by Slag . . . . .	24
F. Conclusions on MgO . . . . .	28
G. Molten Steel Borax Interactions . . . . .	28

CONTENTS (Continued)

VI.	REFRACTORY MATERIALS USED IN FFTF . . . . .	31
A.	FFTf Fire-Retardant Firebrick . . . . .	31
B.	FFTf Insulating Firebrick . . . . .	33
VII.	ANALYSIS OF SPECIMENS FROM EARLIER MOLTEN CORE DEBRIS - CONCRETE EXPERIMENTS AT THE AEROSPACE CORPORATION . . . . .	35
A.	Molten $UO_2$ -HEDL Basalt Concrete Experiments . . . . .	35
B.	Molten $UO_2$ -Magnetite Concrete Experiments . . . . .	39
C.	Molten $UO_2$ -Limestone Concrete Interactions . . . . .	42
D.	Type 304 Molten Stainless Steel-CRBRP Type Limestone Concrete Experiments . . . . .	45
	REFERENCES . . . . .	49

## FIGURES

1.	Iron Oxide-MgO Phase Diagram . . . . .	26
2.	Molten $UO_2$ -Basalt Concrete Experiment . . . . .	37
3.	SEM Photomicrograph of Solidified Molten Uranium Dioxide and Magnetite Concrete . . . . .	41
4.	Molten $UO_2$ -Limestone Concrete Experiment . . . . .	44
5.	Molten Stainless Steel-Limestone Concrete Experiment . . . . .	47



## TABLES

I.	Characteristics of Harklase Brick . . . . .	21
II.	Comparison of the Composition of MgO Brick and Mortar . . . . .	25
III.	Chemical Analysis of Kaiser "Morex" Firebrick . . . . .	31
IV.	Physical Properties of Kaiser "Morex" Firebrick . . . . .	32
V.	Chemical Analysis of A. P. Green G-20 Insulating Firebrick . . . . .	34
VI.	Percentage of Component Oxides in Two Limestone Concretes . . . . .	43

## I. INTRODUCTION

The United States Department of Energy (DOE) is constructing a 400-MWt liquid-metal-cooled reactor facility at Hanford, Washington, to serve as a test bed for breeder-type fuels. This reactor has been designated the Fast Flux Test Facility (FFTF). In order to ensure safe operation, the United States Nuclear Regulatory Commission (NRC) is extensively studying the proposed nuclear power plant system. Some of these studies are concerned with the consequences of postulated accidents in which the reactor core is assumed to melt. In this report, the materials interactions which can occur in this reactor facility are discussed.

In a core meltdown following a hypothetical core disruptive accident, molten fuel debris, consisting of a mixture of  $\text{UO}_2$  and stainless steel from the fuel cladding and the support structures, may melt through the reactor vessel. Various designs have been proposed to contain the molten core either within the reactor vessel or outside of it. If a core-retention system is ultimately required, it is likely that an ex-vessel sacrificial-bed core catcher will be employed. A passive sacrificial bed has the advantage of always being ready in the event of an accident, unlike active systems that may be subject to equipment failure.

A number of sacrificial-bed concepts have been proposed in which materials having desirable thermal, chemical, and mechanical properties, such as MgO brick, are used. However, there is also the possibility that a core catcher may be found to be unnecessary. In this event, the interactions between molten mixtures of  $\text{UO}_2$  and steel with steel-lined concrete must be investigated. The floor of the reactor building will be constructed of reinforced concrete covered with a carbon steel liner whose primary function is to protect the concrete from sodium spills.

This report is an account of work performed for NRC to review and evaluate materials interaction technical information generated during the



course of the FFTF safety review. It is the third of a series of reports prepared for the Office of Nuclear Reactor Regulation.<sup>1, 2</sup> The work also included review of pertinent aspects of the DOE Base Technology Program and the RES Confirmatory Research Program.

In the following sections, experiments performed at Sandia Laboratories and Hanford Engineering Development Laboratory to study the interactions between liquid sodium and basalt concrete will be discussed. Then, experiments conducted at Sandia, in which molten steel was poured into concrete crucibles, will be examined and compared to experiments conducted at The Aerospace Corporation in which molten  $UO_2$  was utilized. In another section, various sacrificial materials that might be used to contain a molten core will be discussed. Refractory materials being used in FFTF will also be reviewed. Finally, the results of analyses of specimens from earlier molten core debris-concrete experiments performed at The Aerospace Corporation will be presented.

## II. SUMMARY

### A. LIQUID SODIUM-BASALT CONCRETE INTERACTIONS

Conflicting results have been obtained in tests at Hanford Engineering Development Laboratory (HEDL) and Sandia. In the HEDL tests, the interactions were mild and there was evidence that suggested the possibility of a self-limiting reaction between sodium and basalt concrete. On the other hand, in several tests at Sandia Laboratories, a vigorous exothermic reaction occurred and all of the sodium was consumed.

The differences may be a consequence of differences in scale. Different water contents may be a secondary consideration. In the larger scale Sandia experiments, cracking and spallation might have caused a greater penetration of sodium into concrete. Since all of the sodium was consumed, there is no way of knowing how far the reaction might have proceeded. Further large-scale, long-term (~100 hr) tests are needed to resolve outstanding issues. Scaling stress analyses need to be performed to determine prototypical geometries and sizes.

### B. MOLTEN CORE DEBRIS - CONCRETE INTERACTIONS

Experiments at The Aerospace Corporation have shown penetration into concrete by molten  $\text{UO}_2$  (~2800°C) at rates as high as 14 cm/hr. Workers at Sandia found that 2800°C molten steel penetrated at a rate as high as 130 cm/hr. The difference is ascribed to the greater thermal conductivity of steel.

With either molten  $\text{UO}_2$  or molten steel, it is expected that melting or thermal erosion will be the principal mechanism for concrete penetration. Chemical attack and spallation will play minor roles when the molten material is far above the melting point of concrete. Further experimentation is needed to examine sustained interactions between molten  $\text{UO}_2$ , molten steel, and various sacrificial materials and concretes. The melt should be kept molten

for a period long enough to achieve quasi-steady-state conditions. Sufficient instrumentation should be provided in order to make an energy balance calculation.

#### C. SACRIFICIAL MATERIALS

It is feasible to delay penetration of molten core debris after a core meltdown and reduce the quantity of gases being evolved into the containment building by the use of sacrificial materials. Sacrificial materials can delay penetration of a molten core by several days, and thereby make effective interdiction of the dose consequences a possibility. A number of potential sacrificial materials are discussed. The best choice of the available materials, when all material and design considerations are taken into account, is MgO.

Possible mortars for use with MgO are also examined. The possibility of attack on MgO by slag from stainless steel is discussed. Finally, experiments with molten stainless steel and borax are reviewed.

#### D. REFRACTORY MATERIALS USED IN THE FFTF

Two kinds of refractory bricks that are being used in the FFTF for the protection of concrete from sodium spills are discussed. Recent experiments to examine the interactions between molten  $\text{UO}_2$  and these firebricks are also reviewed.

It was found that Kaiser "Morex" fire-resistant firebrick, composed principally of  $\text{Al}_2\text{O}_3$  and  $\text{SiO}_2$ , will provide only very limited protection against molten  $\text{UO}_2$  for the concrete floor of the reactor cavity. The observed erosion was considerably greater than that observed in similar experiments with MgO firebricks. The A.P. Green Co. G-20 insulating firebrick, also composed principally of  $\text{Al}_2\text{O}_3$  and  $\text{SiO}_2$ , provides essentially no protection against molten  $\text{UO}_2$  because of its very low density and rapid melting.

E. ANALYSIS OF SPECIMENS FROM EARLIER MOLTEN  
CORE DEBRIS-CONCRETE EXPERIMENTS AT THE  
AEROSPACE CORPORATION

During FY 77, a number of experiments were conducted at Aerospace in which the interactions between molten  $\text{UO}_2$  and concrete were studied. Molten  $\text{UO}_2$  was first poured on a specimen under study to simulate thermal shock. After the specimen cooled, it was placed in another furnace and the  $\text{UO}_2$  was remelted to simulate long-term heating. Results from the analysis of these specimens are presented in this report. The interactions studied include those between molten  $\text{UO}_2$  and HEDL basalt concrete, magnetic concrete and limestone concrete, and between molten steel and limestone concrete.

Of the concretes studied, the two limestone varieties were the most resistant to attack by molten  $\text{UO}_2$ . Although gas evolution was high after contact with molten  $\text{UO}_2$ , the gas was mainly CO and  $\text{CO}_2$ . During the transient segments of the tests, molten  $\text{UO}_2$  adhered to basalt and magnetite concrete but did not adhere to limestone concrete. The lack of adherence might have been caused in part by reduced contact between the molten  $\text{UO}_2$  and limestone concrete as a result of high gas evolution. Also, the layer of limestone concrete in contact with the  $\text{UO}_2$  was reduced to a weak friable mass. This layer in the limestone concrete specimens swelled and crumbled after exposure to air as a result of rehydration.

Magnetite and basalt concrete had a lower resistance to molten  $\text{UO}_2$ . Whereas the gas evolving from magnetite concrete after  $\text{UO}_2$  exposure was a mixture of CO and  $\text{CO}_2$ , the gas from basalt concrete contained a large fraction of hydrogen, which was potentially explosive. For this reason, basalt concrete was felt to be less desirable than the others. More work is needed in this area because there may be other reactions with water vapor from concrete. Neither of the concretes swelled after exposure to molten  $\text{UO}_2$ .

### III. LIQUID SODIUM - BASALT CONCRETE INTERACTIONS

Small-scale experiments in the area of liquid sodium-concrete interactions have been performed in the past for NRC at The Aerospace Corporation.<sup>1, 2</sup> As part of the present study, we were asked to examine the results of experiments conducted elsewhere in this area.

A number of relatively small-scale tests have been performed by HEDL to study the penetration of liquid sodium into magnetite, limestone, and basalt concretes. A smaller number of somewhat larger scale tests to determine the extent of penetration of liquid sodium into limestone and basalt concretes have been carried out at Sandia Laboratories. A considerable effort has been made to understand the interactions between sodium and limestone concrete. However, the results were inconclusive for a variety of reasons. In view of the proposed termination of the Clinch River Breeder Reactor (CRBR), this report will focus primarily on the basalt concrete used in FFTF.

Conflicting results have been obtained by groups at HEDL<sup>3</sup> and Sandia.<sup>4</sup> In the HEDL experiments, 50 lbs of sodium were poured on a number of 1 sq ft specimens at 1600°F. Average penetrations of 1.25 in. after 2 hr, 2.75-3 in. after 8 hr, and 2.0 - 2.5 in. after 24 hr were observed in separate tests. Efforts to conduct longer (100 hr) tests have failed because of various experimental problems. These tests, by themselves, suggested the possibility to HEDL of a self-limiting reaction between sodium and basalt concrete. It was suggested that the reaction was self-limiting because of formation of a hard, brittle protective layer of sodium silicate. However, the HEDL tests have been criticized because of their small scale. HEDL has performed a large-scale test with basalt concrete, but the results have not yet been published; however, based on a meeting with HEDL personnel, the extent of penetration was very limited. Aerospace will evaluate these data as they become available.

Tests on a larger scale were conducted at Sandia.\* In test 7, 45 kg of sodium at 485°C was poured in a basalt concrete crucible. The results seem to support the HEDL conclusion because the test was quiescent, with no evidence of concrete spallation or an exothermic reaction. This test, however, used a New Mexico basalt aggregate concrete rather than Columbia River basalt aggregate concrete and was conducted at a lower temperature than desired. When the experiment was repeated at 520°C in a FFTF type basalt concrete crucible, the temperature in the sodium pool remained constant for about 80 min and then rose to 780°C, indicating an exothermic reaction. Although the crucible was filled to a depth of 13 in. initially, all sodium present was consumed in the reaction before the test ended so that it is not possible to determine how far penetration might ultimately have proceeded had sufficient sodium been used.

Post-test examination showed that downward penetration extended 1.75 in. into the concrete and that sidewall penetration extended as far as 5 in. along cracks. More sidewall attack occurred where cracks were observed, probably because of a greater surface area in the cracked regions. This allowed greater diffusion of water into the pool from the crack.

The conflicting results obtained at Sandia and HEDL could also be a result of scale effects which resulted in different stress fields in the concrete. Differences in chemistry arising from different water contents could also cause conflicting results. The only known contributor to a difference in chemical environment between the two series of tests is the water content.

The water content of the concrete seems to be an important contributor to the exothermic reaction because of the sodium-water reaction. Unfortunately, the water content of the concretes used in these experiments has been determined by use of the slump test commonly employed in the construction industry.

---

\*This report covers only Sandia tests 1 through 12. Details of later tests were not available at the time this report was prepared.

While this may be a good field test, it is inadequate in phenomenological studies where the chemistry of concretes prepared at different localities is being compared. The HEDL and Sandia basalt concretes may have substantially different water contents even though they both had approximately the same slump test results.

The only other available sodium-basalt concrete test data are the results of a small-scale test performed at The Aerospace Corporation several years ago in which a 4.8-cm dia, 7.6-cm long cylinder of HEDL basalt concrete was totally destroyed by only 114 g of sodium at 550°C. At that time, it was suggested that the water content of the concrete and the sodium-water reaction were responsible for the observed behavior. Small-scale scoping tests such as those are useful in obtaining information on chemical compatibility. However, small-scale tests will not resolve geometric and scale dependent issues, such as simulating stress fields in the concrete including cracking and spallation.

It is clear that additional large-scale tests are needed to resolve the conflicting results of early tests. The tests should be long term (~100 hr) and there should be an excess of sodium present. Scaling stress analyses should be performed to determine the most prototypical geometry which simulates the FFTF reactor cavity configuration. Large-scale tests are desirable because of a concern that the differences between the results observed at HEDL and Sandia may be a consequence of different geometries and stress fields, including cracking and/or spallation. Since the liquid sodium was at a temperature below the melting point of the concrete, there is the suggestion from liquid sodium tests with other concretes that both cracking and spallation may be important contributors to the erosion of basalt concrete. Both cracking and spallation are scale and geometry dependent.

Other concerns about these test results center on the geometry and the way in which specimens are restrained. Square specimens such as those used at HEDL will be subjected to greater stress at the corners than the cylindrical

specimens used at Sandia. When the mechanical response of concrete to reactions with sodium is examined in greater detail, the manner of restraint must be considered. Restraints will alter the stress field in the specimen and thereby affect the extent of cracking and spallation. Cracking and spallation might increase in larger specimens because of the restraining effect of the larger volume of material. In small-scale tests, no portion of the specimen is very far from a wall. Thus, the material in the center is not as rigidly restrained as in a larger specimen so that stresses will not build up rapidly. In a larger specimen, material in the center is far from the walls and will be rigidly restrained by its surroundings, thus increasing the chances of spallation and cracking to reduce stress. In one large-scale test at Sandia (No. 12), erosion was much enhanced in regions where cracking was observed. This increased erosion probably resulted from the crack-induced increase in surface area available for attack by liquid sodium.

The presence of rebars in the actual concrete construction system is another cause for concern. The extent of penetration might be increased by rebar-induced cracking. This cracking is expected from differential thermal expansion between the steel and concrete and from enhanced thermal conduction into the concrete.

Another area of concern in the HEDL tests is the use of the same sodium pool depths in all experiments. It is observed that shallow sodium pools produce significantly greater penetration than deep pools. It is believed that NaOH from the reaction between sodium and water driven from the concrete by heat is responsible for much of the penetration that occurs. Attack by NaOH is facilitated by the formation of a separate layer of NaOH when the sodium layer becomes saturated with NaOH. In a deeper sodium pool, the NaOH layer takes much longer to form. Also, in deeper sodium pools, the reaction products may be diluted with sodium, thereby lowering the viscosity of the protective layer and allowing sodium to diffuse through the layer more readily. It is also possible that a sodium silicate protective layer may not



form until the sodium pool is saturated. If the pool depth is increased, the protective layer would form later, leading to increased penetration. It should be kept in mind that these hypotheses are speculative and suggest a behavior for the reaction product layer which is unconfirmed. It is not known at this time whether pool depth is a significant factor. However, it is hoped that some of HEDL's experiments in the future will employ different pool depths to resolve this question.

With greater pool depth, hydrostatic pressure in FFTF (8 psi at the bottom of the pool) may force the sodium into cracks in the concrete. It is probable that the gas evolving would be under sufficient pressure to force any sodium out of the cracks. In fact, data from Sandia and HEDL (Sandia Nos. 1-5, HEDL-SC-1-12) suggests that the evolving gas did force sodium out of the crack in these tests.

A final area of concern about the HEDL tests is that all were performed at a single temperature, near the boiling point of sodium. Some tests should have been performed at lower temperatures to ensure that the reaction kinetics were not being forced to go in one direction by the high temperature. At lower temperatures, different chemical reactions may be dominant. HEDL did perform some lower temperature experiments but these included sodium hydroxide in addition to sodium. Some lower temperature tests without sodium hydroxide would also be desirable. Although it seems probable that the high-temperature case is the worst one, most of the high penetration reactions started at the relatively low temperature of 550°C.

#### IV. MOLTEN CORE DEBRIS-CONCRETE INTERACTIONS

In a hypothetical core disruptive accident, molten core debris may come into contact with the concrete floor of the reactor cavity. If this occurs, there are two fuel debris configuration scenarios, a coolable debris bed or molten fuel in contact with the concrete. In the coolable debris bed scenario, the core debris freezes and fragments on contact with the liquid sodium. The concrete will then be principally attacked by sodium. In the other scenario, if the debris is unevenly distributed, it may remelt due either to decay heat or recriticality, and this would expose the concrete to molten fuel. The concrete may also come into contact with molten fuel if the fuel does not fragment because it reaches the concrete first, before the sodium. We do not believe that it is possible at this time to say with confidence that the core debris will be spread in a coolable configuration; therefore, molten pool configurations must also be considered.

##### A. MOLTEN UO<sub>2</sub>

If a coolable debris bed does not form, experiments at Aerospace show penetration into concrete by molten UO<sub>2</sub> at the rates of 5.5 in./hr for basalt concrete, 2.4 in./hr for magnetite concrete, and 1.0 in./hr for limestone concrete. In these experiments, the applied integrated power was 12.5, 13.4, and 6.25 KWHR, respectively. These penetration rates are subject to some qualifications. The UO<sub>2</sub> was heated by an electric arc and it is not possible to say what fraction of the applied power was coupled into the material. The heat transfer depends on the radiative coupling between the plasma and molten material and the conductivity of the liquid phase. If the coupling is similar for each concrete, since the integrated powers were similar, basalt would seem to be least resistant to penetration by UO<sub>2</sub>. Another qualification is that the area of the molten UO<sub>2</sub> pool heated was only about 1.5 in. in diameter. In order to heat the entire quantity of UO<sub>2</sub>, the operator moved the electrode over the entire UO<sub>2</sub> pool. Consequently, the entire pool may not have been molten at all times.

Melting of concrete by molten  $\text{UO}_2$  and steel, rather than spallation or chemical attack, was the principal mechanism of concrete erosion. When one compares molten steel and  $\text{UO}_2$ , it can be argued that heat transfer from high-temperature molten steel will dominate concrete erosion because of its higher thermal conductivity relative to  $\text{UO}_2$ . Although this seems probable, molten  $\text{UO}_2$  will also be an important factor in concrete erosive processes, particularly in the early stages of a core meltdown event, when it will be in contact with the concrete because of its high density. Molten  $\text{UO}_2$  will interact with concrete by forming low melting eutectic mixtures. Molten steel and molten concrete, on the other hand, are relatively immiscible and will not form a low melting mixture. In addition, the temperature of the molten steel is limited by its boiling point, approximately  $2700^\circ\text{C}$ . Molten  $\text{UO}_2$ , however, with its higher boiling point, may attain a higher temperature in a core meltdown than molten steel, which may offset its lower thermal conductivity.

#### B. MOLTEN STEEL EXPERIMENTS

The molten steel experiments at Sandia were of two types. In the first category, quantities of steel weighing up to 200 kg were heated by induction to  $1700^\circ\text{C}$  and poured into concrete crucibles. In the second type of experiment, 10-12 kg of high temperature ( $2700^\circ\text{C}$ ) molten steel were prepared by a thermite reaction within a 12 cm diam cavity in a concrete specimen.

It was concluded from the molten steel experiments that the principal mechanism in concrete erosion is the melting of the concrete rather than spallation or chemical attack. The penetration rates were found to be relatively independent of the aggregate types used in the concretes, and melting of the binding material was the principal mechanism of erosion. At  $1700^\circ\text{C}$  in the large-scale tests, the penetration rates were found to be  $25 \pm 15$  cm/hr and, at  $2800^\circ\text{C}$  in the small-scale tests, the penetration rates were  $130 \pm 50$  cm/hr. Although the penetration rates are quoted at specific temperatures, these are only the initial experimental temperatures. Since the molten mass presumably cooled rapidly in both the small and large-scale experiments, the

average temperature over the period during which the steel was molten was less than indicated. This suggests that these penetration rates are non-conservative.

These penetration rates are significantly larger than the penetration rates for sodium into concrete at 800°C reported in experiments at HEDL and Sandia. If molten steel comes into contact with concrete, these experiments suggest that the consequences will be serious. There are several reasons for the greater penetration rate for molten steel into concrete as compared to sodium. The molten steel is at a temperature above the concrete melting point so that erosion is by melting rather than by chemical means or spallation. Furthermore, the high density of the steel causes the concrete slag to float to the top of the molten steel. There can be no protective layer of reaction products as in the sodium-concrete experiments and, consequently, fresh concrete is continually exposed to the molten steel.

The very high penetration rates observed for molten steel as compared to molten  $\text{UO}_2$  are probably due to the greater thermal conductivity of the molten steel (relative to molten  $\text{UO}_2$ ).

The extent of the melt penetration is a function of the difference between heat generated within the melt and the heat losses from the melt. These heat losses include the enthalpy required to heat the concrete to its liquidus temperature and any endothermic reactions occurring in the concrete. For a melt of a given heat capacity, basalt concrete is eroded to a greater depth than limestone concrete because of its lower enthalpy.

Gas generated in limestone concrete insulates the concrete from the melt and carries away heat that might have been transferred into it. The ratio of horizontal to vertical heat fluxes from the melt to concrete was found to be an inverse function of the gas generation rate. This ratio for limestone, which has a high gas generation rate, was 1:7 while for basalt concrete it was 1:3. We suggest that this behavior occurs because the gas film can serve as an

insulator between the melt and the concrete. The gas leaving the bottom of the cavity flows upward through the melt and is only present briefly at the surface of the concrete. On the other hand, the gas generated near the bottom of the sidewalls remains in close proximity to the wall for a relatively long time as it rises and thus provides an additional insulating film. As a consequence, a deeper, narrower cavity should be formed in limestone concrete as it generates the most gas for the same total amount of concrete decomposition.

Concrete penetration is thought to be only insignificantly affected by spallation, accounting for no more than 0.5 cm in a wide variety of concretes including basaltic concretes. This appears to be true of almost all the experimental data presented thus far in which higher temperature melts were used. Even though some small-scale spallation was noted, typically in the first few millimeters, it was only observed initially during the heating of a fresh concrete surface. When specimens were exposed to molten steel for a second time, no spallation occurred. A considerable amount of cracking in the concrete was observed in the large-scale steel tests, but steel was not observed in the cracks. The cracks apparently provided a pathway for water vapor and gases to escape from the concrete.

### C. GAS GENERATION

Gases generated during the melt-concrete interaction are the result of the thermal decomposition of hydrates and carbonates within the concrete or are the consequence of the heat induced expulsion of air from pores in the material.

Gases released from basaltic concrete in the steel-concrete tests at Sandia were found to be quite similar to the gases released from limestone concrete even though limestone concrete has 50% more gas-generating species per unit volume of concrete. (We have not had access to the Sandia gas analysis data for each experiment.) This reported result seems surprising in view of

the large evolution of  $\text{CO}_2$  from carbonates in the limestone concrete. One would expect a large evolution of both  $\text{CO}_2$  and water from limestone aggregate above  $600^\circ\text{C}$  and water only from basalt aggregate.

Gases liberated from the concrete are chemically reduced to hydrogen and carbon monoxide as they pass through the metallic portions of the melt. Once above the melt, some of these gases may recombine to form hydrocarbons. This reaction should be enhanced by the presence of nickel aerosols from the stainless steel. Finely divided nickel will be formed from the  $\text{Ni}(\text{CO})_4$  produced when CO is passed through hot nickel. The reduction of water and  $\text{CO}_2$  does not necessarily go to completion under the conditions of a melt-concrete interaction. When bursts of gas are generated, the gas comes through the melt only partially reduced as indicated by greater concentrations of  $\text{CO}_2$ .

Oxidation of metallic portions of the melt is not an unlimited process. Eventually, in a closed system, chemical equilibrium is attained and the reverse reactions occur. However, the chemical equilibrium will probably strongly favor oxide over metal formation.

#### D. FISSION PRODUCT DISTRIBUTION

Redistribution of fission products from the metallic portion of the melt into the oxide phases will probably occur. This is expected if the fission products have oxidized. In principle, the concentration of fission products in each phase can be calculated from the Nernst distribution equation.

Aerosol generation was reported to be extensive and dependent on melt temperature and gas generation rates in tests at Sandia. Substantial aerosols of  $\text{UO}_2$  have also been generated in experiments using electric arcs at Atomics International and The Aerospace Corporation. Aerosol generation is not well understood at present. Aerosols are expected from both non-fuel (steel) and fuel sources.

## E. SCALING CONSIDERATIONS

Some interesting generalizations can be made about the factors important in scale-up from the size of the present experiments to a full-size reactor. First, concrete decomposition and melting chemistry are insensitive to experimental scale provided that care is taken to make careful selection of the small representative samples. This is a result of experiments in which no significant spalling was observed because of the dominance of melting over other processes.

Second, gas reduction by the molten steel is scale dependent. Since gas reduction depends strongly on the length of time the gas is in contact with the melt, a deeper pool would tend to complete the reduction reactions. In these tests, water was reduced causing free hydrogen to be generated. In some of the small-scale tests, however,  $\text{CO}_2$  was not completely reduced to CO.

Third, heat and mass flow behavior is both scale and geometry dependent. Mass transport appears to be the result of a gas-driven convection system. In addition to the removal of molten debris from the concrete surface, this convection system also tends to keep the entire steel mass at a uniform temperature. Also important is the effect of the pool depth on the gas blanket which tends to form at the steel-concrete interface. A deeper pool would be expected to reduce the thickness of this gas layer and increase heat transfer. Furthermore, with higher pressures it might be expected that the melt might be forced into cracks that form in the concrete. This might be simulated experimentally by pressurizing the volume above the melt.

## V. SACRIFICIAL MATERIALS

### A. DESIRABLE PROPERTIES

There are a number of considerations in the choice of a sacrificial material to either contain a molten core indefinitely or to delay melt-through penetration through the containment basemat. Desirable characteristics for a sacrificial material include the following:

1. High melting point. This is desirable in order to reduce the rate of advance of the melting front of core material into the sacrificial bed material.
2. High specific heat and heat of fusion. These properties are desirable in order to reduce the rate of advance of the melting front by absorbing heat from the molten core debris.
3. Low thermal conductivity. This will also reduce the rate of advance of the melting front by slowing the rate of transmission of energy into the sacrificial bed material.
4. High density. If the sacrificial material has a high density, it will not float to the surface of the melt if core material gets underneath it by way of cracks, seams, or flaws.
5. Miscibility of molten fuel and sacrificial layer. If the fuel and sacrificial material are miscible, the volumetric heating rate of molten fuel will be decreased substantially by dilution.
6. Chemical compatibility with molten core debris. The sacrificial material should not react chemically with molten  $\text{UO}_2$  or steel. It is especially important that no exothermic reactions occur between the sacrificial material and the molten core debris. It is also important that the sacrificial material not form very low melting temperature compounds when exposed to the molten core material.
7. No gases should be generated. Gaseous reaction products, such as  $\text{CO}$ ,  $\text{CO}_2$ , and  $\text{H}_2$ , should not be generated by chemical reactions between the molten core debris and sacrificial materials. The generation of these gases can create a potential for an explosion and increase the sparging of fission products from core melt debris.



8. Resistance to thermal shock. A desirable characteristic of the sacrificial material is that it be sufficiently resistant to thermal shock so that it does not fail mechanically when exposed to the rapid heating transient of a hypothetical core meltdown accident.
9. Pre-accident stability. The sacrificial bed should be stable in the environment of the reactor cavity for the expected life of the reactor.
10. Limited neutron moderation. The sacrificial material must not increase the potential for recriticality of the core material. Neutron absorbers, such as tantalum and boron, could be added to alleviate this concern.
11. Low cost and availability. It is highly desirable that the sacrificial material be of low cost and that a technology exist for manufacturing mechanically stable structures, such as bricks, or larger cast structures from this material at reasonable cost.

## B. AVAILABLE MATERIALS

Of all known high-temperature materials, only a relatively few have been studied sufficiently so that an extensive body of engineering data is available. While in many cases there is insufficient experimental data to make generalizations, it can be stated that oxides are more likely to be stable chemically in the presence of molten  $\text{UO}_2$  than carbides, borides, and nitrides. These latter materials tend to oxidize, especially in the presence of excess oxygen. In general, oxides have only minor chemical reactions with molten core debris. The oxides typically form eutectic mixtures with  $\text{UO}_2$  which have melting points below that of either pure constituent. The oxides of magnesium ( $\text{MgO}$ ) and aluminum ( $\text{Al}_2\text{O}_3$ ) are used for crucible liners in the steel industry and consequently are excellent for the containment of molten steel. A few of the better refractory materials are discussed in the following paragraphs.

Magnesium oxide ( $\text{MgO}$ ) has the advantages of a very high specific heat (0.31 cal/g°C), a high melting point (2800°C), excellent stability with respect to molten  $\text{UO}_2$  and steel, ease of fabrication and relatively low cost.

In large quantities, relatively pure Harklase MgO bricks are available at a cost of approximately \$1.80 each for a 6 kg standard size brick with dimensions of 9 in. × 4-1/2 in. × 2-1/2 in.

The principal disadvantage of MgO, which is also a disadvantage for titanium carbide (TiC), aluminum oxide ( $\text{Al}_2\text{O}_3$ ), and graphite, is that it has a low density compared to  $\text{UO}_2$  and would tend to float in the molten core debris. Some method has to be developed to prevent the MgO from floating away into the denser molten core material. The MgO bricks could probably be held in place by constructing a bed of many layers of bricks. The bricks could be wedged together to form an inverted arch with an interlocking, tongue-in-groove design.

Graphite has the advantages of a high sublimation temperature, good specific heat, easy fabrication, and low cost. It has two serious disadvantages however. It acts as a neutron moderator and thus increases the potential for recriticality. The reactions of graphite with  $\text{UO}_2$  generating CO,  $\text{CO}_2$ , and UC are not completely understood and may be potentially serious problems.

Titanium carbide (TiC) has a very high melting point ( $3076^\circ\text{C}$ ), good specific heat ( $0.21 \text{ cal/g}^\circ\text{C}$ ), and is available at reasonable cost. However, it has a low density, marginal chemical compatibility with respect to molten  $\text{UO}_2$ , and it is difficult to fabricate, requiring high temperature inert atmosphere facilities for the production of bricks. These production facilities do not currently exist.

Zirconium oxide ( $\text{ZrO}_2$ ) has the advantages of a high melting point ( $2730^\circ\text{C}$ ) and density. It is chemically stable with respect to molten core debris. Its disadvantages include a low specific heat, structural instabilities, and high cost.

Aluminum oxide ( $\text{Al}_2\text{O}_3$ ) has a high specific heat, is chemically stable with respect to molten core debris, and is available at relatively low cost. However, it has a low density and melting point ( $2037^\circ\text{C}$ ).

### C. MAGNESIUM OXIDE

After considering a number of candidate sacrificial materials in view of the above materials consolidations, MgO appears to be the best candidate material. It is possible that some less well-known material might serve as a better sacrificial layer; this, however, would probably require an extensive research and development program. It is not obvious at this time that any other material would offer any significant advantages.

Table I lists the properties of a good quality MgO brick; it is important to obtain high-quality MgO because impurities can significantly degrade high-temperature performance. This particular material was manufactured by Harbison and Walker Refractories and is sold under the name "Harklase." The advantages of MgO, as mentioned earlier, include a high melting temperature, high heat capacity, low thermal conductivity, high degree of chemical compatibility, resistance to thermal and mechanical shock, ease of fabrication and low cost. There are no adverse chemical reactions and gas evolution is very limited, consisting mainly of gas forced out of the pores in the material. MgO has been used in the steel industry for many years and, consequently, its properties at high temperatures are relatively well understood.

MgO (melting point  $\sim 2800^{\circ}\text{C}$ ) and uranium oxide (melting point  $\sim 2850^{\circ}\text{C}$ ) are miscible in the liquid state and form liquid solutions with a eutectic composition of about 50 mol % MgO (13 wt%) in  $\text{UO}_2$ . The reported eutectic melting temperatures range from about 1800 to  $2300^{\circ}\text{C}$ , with the higher temperatures occurring in oxygen-free surroundings.

Some differences have been observed in the rate of solubility of  $\text{UO}_2$  into MgO. Meacham<sup>5</sup> reported formation of a  $\text{UO}_2$ -MgO eutectic at  $2375^{\circ}\text{C}$  with rapid, complete solution of all of the  $\text{UO}_2$  present in three minutes. The  $\text{UO}_2$  and stainless steel in his experiment were placed in a cavity only 0.64 cm in diameter by 1.27-cm deep. In his relatively small experiment, diffusion and stirring effects would not be expected to be important.

Table I. Characteristics of Harklase Brick

Quantitative Chemical Analysis		Semiquantitative Chemical Analysis	
<u>Compound</u>	<u>Percent</u>	<u>Element</u>	<u>Percent</u>
SiO <sub>2</sub>	0.7	Al	0.1
Fe <sub>2</sub> O <sub>3</sub>	0.4	Ca	0.1
MgO	96.3	Mn	0.01
SO <sub>3</sub>	0.03	Ti	0.05
Bulk density	= 2.72 g/cm <sup>3</sup>		
Average void volume	= 16.94%		
Melting point:	2850°C		
Specific heat:	0.31 cal/g°C		

In a larger scale experiment, Stein et al.,<sup>6</sup> reported that part of a magnesia specimen dissolved smoothly into molten UO<sub>2</sub> in the range 2200-2300°C over a period of 26 min. In this experiment, 9.5 kg of UO<sub>2</sub> was used and the MgO specimen was a rectangular solid with a thickness of 2.5 cm and a length and width of 10 cm.

In experiments at The Aerospace Corporation, Swanson et al.,<sup>7,8</sup> found that the rate of erosion of MgO brick seemed to be influenced by the degree of stirring of the molten UO<sub>2</sub>. Penetration of 0.6 cm in 5 min was observed when 100 g of UO<sub>2</sub> were vigorously stirred by an electric arc. Under more quiescent conditions, with 2 kg of UO<sub>2</sub> on an 8.9 cm diam cylinder with a thickness of 7.6 cm, erosion occurred much more slowly with a diffusion coefficient of only  $1.5 \times 10^{-5}$  cm<sup>2</sup>/sec. In the latter experiments, the UO<sub>2</sub> was cooler than in the vigorous stirring experiment, but

it is believed that it was molten in the region in contact with the MgO. The difference between the experiments seems to be a consequence of stirring in the first experiment bringing fresh molten  $\text{UO}_2$  in contact with the MgO.

In both of the Aerospace experiments,<sup>7,8</sup> three layers were observed consisting of a mixture of a eutectic composition of  $\text{UO}_2$  and MgO in  $\text{UO}_2$ , a layer of  $\text{UO}_2$  attacking the MgO binder and grains, and finally a layer of MgO. Molten  $\text{UO}_2$  preferentially attacked the low melting phase binding the MgO grains and then formed a hypoeutectic mixture with melted MgO.

When molten  $\text{UO}_2$  was poured on an MgO brick in the Aerospace experiments to simulate thermal shock, there was little sign of interaction except for a discolored region extending 1 cm into the brick. Thermal-shock cracks that formed on cooling, after solidification of the  $\text{UO}_2$ , extended 2 cm into the material. Although MgO is not usually considered a thermal-shock-resistant material, under these conditions, it performed acceptably. It should be noted, however, that the MgO brick was coated with  $\text{UO}_2$  dust generated as an aerosol by the electric arc employed to heat the  $\text{UO}_2$ . This insulating coating may have reduced the transfer of thermal shock and heat. The possibility of such an effect suggests that placing layers of powders or larger particles composed of such materials as MgO on top of a layered brick configuration could be used to effectively reduce the initial thermal shock.

Under the experimental conditions of the Aerospace experiments, the MgO performed adequately as a container material for molten  $\text{UO}_2$ . There was some attack, but it was relatively minor and thermal shock effects were small.

The low density of MgO relative to molten  $\text{UO}_2$  gives rise to the possibility that molten  $\text{UO}_2$  may undermine a sacrificial layer by flowing under the bricks and floating them away. However, in a typical installation, such as in steel mills, the bricks are placed with spaces between them to allow for thermal expansion. When hot metal comes in contact with the

bricks, they expand forming a tight structure which the metal is unable to penetrate. Consequently, movement of molten metal through the joints into successive layers of bricks is not considered to be a problem.

Design of a sacrificial bed composed of layers of these bricks may be complicated by the variation in the temperature of the constituents of the molten core debris. Normally, in the design of a steel furnace, the joint spacing is designed to contain a hot material at one specific temperature. In order to retain molten core debris, the joint spacing between bricks must be large enough to accommodate expansion of the bricks at the highest expected temperature, probably about 2800°C, the temperature of molten  $\text{UO}_2$ . However, some constituents of the molten core debris may be much cooler, consisting, for example, of molten iron and solidified  $\text{UO}_2$ . Such a mixture might leak through a structure with joints designed to retain molten  $\text{UO}_2$  and cause flotation of the bricks. On the other hand, if the joints are spaced with lower melting core debris in mind, the core retention structure may be damaged by crushing caused by thermal expansion if higher than expected temperatures are encountered. A design consisting of many layers of bricks wedged into an inverted spherical dome would probably ensure that they remain in place. Further investigation is needed in this area.

#### D. MORTARS FOR USE WITH MgO

With any core retention material, there is a question about what should be done at locations where penetrations are required or at corners, edges, etc. A mortar, "Oxybond," has been developed for use with "Harklase" MgO bricks in high-temperature applications and should work well in these regions, based on information supplied by the vendor. The mortar is not intended for use between bricks. Introduction of mortar into the joints between bricks would cause the brick structure to be destroyed by the pressure generated during thermal expansion.

Oxybond has a somewhat lower melting temperature than MgO (about 50°C lower) and is made from a dry mix consisting of hard fired magnesia fines, or from crystals, below number 325 mesh. Hard fired MgO is material that has been heated to the point where amorphous MgO is converted to small periclase crystals. Oxybond sets in place or sinters when heated to above 2000°C. Since the mortar employed around any penetrations has a lower melting point than the MgO bricks, it would be preferentially attacked by hot core debris. Consequently, minimal use should be made of the mortar, and penetrations in the structure should be kept to a minimum. No experiments have been performed to date with molten  $UO_2$  and this mortar.

A second kind of mortar is also manufactured by Harbison and Walker Refractories for use with Harklase MgO firebricks. This mortar, sold under the name "Peribond," can only be used at temperatures up to 1600°C, and consequently it is not suitable for use as a core retention material. In addition, Peribond mortar is mixed with water and is air setting. It should not be used in applications where it may come in contact with liquid sodium because of the retained water employed during mixing. As Oxybond mortar is a dry mix, it can be used with sodium. Table II lists the compositions of each mortar and compares them to Harklase brick. Peribond mortar is relatively impure and contains a large quantity of silica. The composition of Oxybond mortar, as shown in Table II, is more similar to Harklase brick than is the Peribond mortar. The lower silica concentration is responsible for the higher melting temperature of the Oxybond mortar.

#### E. EROSION OF MgO BY SLAG

During one experiment at Sandia, molten steel at 1700°C was heated in an MgO crucible in air. Slag formed on top of the steel and was observed to attack the MgO. The phenomenon has been described as "slag line attack" by Sandia. An erosion rate was observed of 1 in. in 3 hr. This was ascribed to a low melting eutectic between iron oxide and MgO at 1591°C. A phase

Table II. Comparison of the Composition of MgO Brick and Mortar (percent by weight)

	Harklase Brick	Peribond Mortar	Oxybond Mortar
MgO	97.9	79.0	94.0
SiO <sub>2</sub>	0.8	14.7	4.2
CaO	0.6	1.1	0.9
Al <sub>2</sub> O <sub>3</sub>	0.4	2.4	0.3
Fe <sub>2</sub> O <sub>3</sub>	0.2	0.8	0.3
Alkalies		2.2	

diagram for the iron-oxide MgO system is shown in Fig. 1. It was suggested that this erosion rate could lead to the failure of a MgO sacrificial layer if one is employed to protect concrete from molten core debris.

We believe that the erosion observed in this test represents the total erosion that should be expected at this temperature rather than an erosion rate. When molten steel comes in contact with oxygen in either air or a 2%O<sub>2</sub>-98%N<sub>2</sub> atmosphere, a layer of iron oxide slag will form and float on top of the molten iron. This iron oxide will dissolve MgO from the side-walls until the iron oxide-MgO mixture has the composition shown by the phase diagram at the temperature of the slag. At 1700°C, the saturated mixture will contain 10% MgO and, at 2000°C, it will contain 26% MgO. When the saturation concentration is reached, dissolution of MgO by iron oxide will cease. The total amount of MgO that dissolves will be relatively small because the slag layer will be thin and because of the relatively small quantity of MgO in solution at saturation. As the temperature of the mixture is increased, the extent of erosion will also increase, as given by the phase diagram. Since the slag layer will shield the molten iron metal underneath



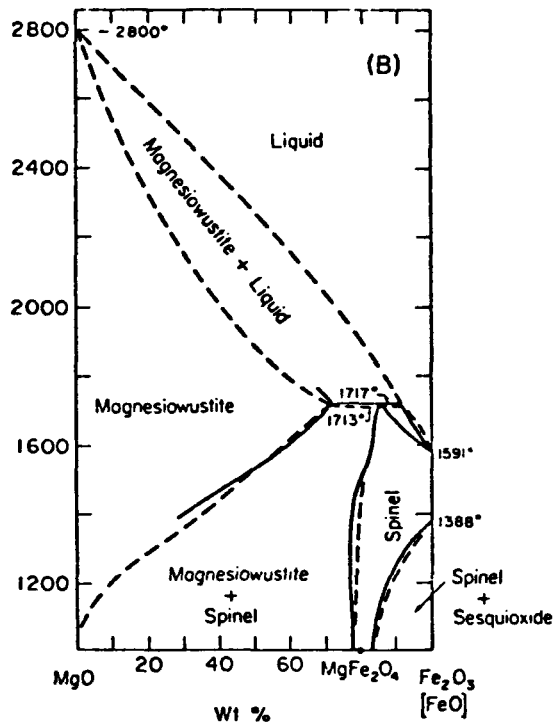


Fig. 1. Iron Oxide-MgO Phase Diagram

from further attack by oxygen, no additional iron oxide will form and, consequently, no further erosion of the MgO sidewall will occur. As iron oxide and iron have very limited miscibility and the oxide floats on top of the metal, the slag will remain in place as a protective layer unless the steel is vigorously agitated, as by boiling (boiling point = 2750°C). Iron will not attack MgO directly unless it is above the melting point of MgO (2800°C) because molten iron and MgO are immiscible.

It should be noted that the extent of sidewall erosion will increase with the amount of slag which, in turn, increases with cavity diameter. One approach to this problem would be to leave loose MgO bricks on top of the MgO structure. In the event of an accident, these bricks would float to the top of the molten pool and saturate the slag layer. Crushed MgO could be used to serve this purpose and also to protect the MgO brick from thermal shock.

A representative of Harbison and Walker Refractories, manufacturers of Harklase MgO, indicated that slag line attack did not represent a problem at either 1700°C or 2000°C. He based this conclusion on their past experience with steel manufacturing operations.

The oxides of nickel and chromium also form low melting eutectics with  $\text{UO}_2$ . However, these eutectics are close in temperature to the  $\text{UO}_2$ -MgO eutectic. Consequently, the iron oxide-MgO eutectic is expected to be the worst case.

In summary, the erosion observed during the test at Sandia was probably the total erosion that can be expected at this temperature rather than an erosion rate. Erosion will occur, but it will be limited by the small amount of slag present and the saturation composition of the mixture on its phase diagram at each temperature. However, it should be noted that impurities in the MgO may substantially alter the expected behavior.  $\text{SiO}_2$  and  $\text{Al}_2\text{O}_3$  impurities in MgO, if present in substantial quantities, can lead to the formation of complex three- or four-component mixtures with low melting points.

#### F. CONCLUSIONS ON MgO

In conclusion, it is believed to be feasible to delay substantially the penetration of molten  $\text{UO}_2$  after core meltdown. Without a protective sacrificial refractory material, molten core debris would very quickly penetrate the unprotected concrete layer of the containment basemat. However, with a protective sacrificial refractory material, such as MgO, it is estimated that times of the order of a week would be required before penetration occurs, for typical containment building concrete basemats. This time delay would make effective interdiction of the dose consequences possible. Furthermore, as previously indicated, MgO is inexpensive, readily available and easily fabricated. Its properties are relatively well understood. It seems to be the best choice among the available sacrificial materials when all of the design considerations are taken into account.

#### G. MOLTEN STEEL BORAX INTERACTIONS

Sandia is examining the effects of molten steel on borax, FFTF firebrick, MgO and high alumina cement. The purpose of the program is to examine alternative core retention or core dilution materials for the protection or replacement of conventional concrete.

A borax system has been proposed for use in the containment of molten cores. Unlike refractory systems, which would contain a molten core in a high melting temperature crucible, this material would contain molten core debris by diluting it in a large volume of low melting temperature, high heat capacity material. The chances for recriticality would be reduced since boron has a high neutron capture cross section and the fuel and diluent (borax) are completely miscible. Eventually, when a large quantity of borax is dissolved by the fuel, the mixture should freeze. However, molten steel will not dissolve in borax, and will remain in a separate layer.

The borax ( $\text{Na}_2\text{B}_4\text{O}_7$ ) would be cast into bricks which would be sealed in steel cans in order to protect them from dissolution by moisture. Borax has a melting point of  $741^\circ\text{C}$ , a boiling point of  $1570^\circ\text{C}$ , and a density of

2.3 g/cm<sup>3</sup>. Its advantages include its low cost and its ability to absorb neutrons, thereby reducing the potential for recriticality.

In a transient experiment performed at Sandia, 200 kg of molten stainless steel was poured into a 13-in. deep, 13-in. diam cavity in a one-ton borax crucible. At 1700°C, the transient interactions between borax and molten steel were very mild. Molten steel was unable to penetrate the borax because of its high heat capacity. The borax remained molten for approximately three hours. Since the borax was above its melting point, some of it decomposed into boric oxide.

Several possible problems are anticipated with this material if it is employed to contain molten cores. The most serious problem concerns the interaction between borax and molten core debris at 2700°C, more than 1100°C above the boiling point of borax. If molten core debris can transfer heat into borax fast enough, a vapor explosion is possible. Whether this will occur depends on the relative thermal conductivities of the materials at these extremely high temperatures. Reliable data for calculations in this temperature regime probably do not exist. Experiments with high temperature (2700°C) molten core debris and borax are needed before this material can be seriously considered. While the dilution concept has merit, materials with such low boiling points should be avoided unless it can be shown that an explosion will not occur. The substantial gas generation that would be expected also poses problems for the containment building.

Another area of concern arises because of the low-melting point of the borax. The high density of steel and its immiscibility in borax would cause the steel present in the reactor to fall to the bottom of the molten pool where it would be in contact with the solid borax layer. It is possible that a stream or jet of molten steel could excavate a hole in the borax layer and eventually penetrate it entirely before solidifying.

Sandia's test results suggest that penetration will not occur and that the interactions are mild, at least with relatively low-temperature molten

steel. However, in a hypothetical core disruptive accident, the core debris will be much hotter and will be generating heat from radioactive decay. The decay heat will enhance the penetration of the molten core debris into the borax and could lead to rapid penetration.

In view of the low-melting point of borax, it probably would be best to use this material in a two-material system with a layer of borax covering a more refractory material. In this way, if it can be shown that there is no vapor explosion problem, and no significant gas generation, it would be possible to take advantage of the properties of borax as a dilutant without sacrificing protection against rapid penetration.

## VI. REFRACTORY MATERIALS USED IN FFTF

### A. FFTF FIRE-RETARDANT FIREBRICK

A layer of fire-retardant firebrick will be used between the low-carbon steel liner and the insulating firebrick at FFTF. "Morex" firebrick manufactured by Kaiser Refractories at Mexico, Missouri, has been proposed for this purpose.

The brick is mustard colored containing white, beige, pink, and gray particles. Numerous cracks and pores are visible and the material appears to be hard and brittle. A porosity range of 15 to 19% has been reported by the manufacturer. Its bulk density range is reported to be 2.13 to 2.19 g/cm<sup>3</sup>.

The results of a chemical analysis of the brick are shown in Table III. As in the case of the insulating brick, the principal constituents are SiO<sub>2</sub> and Al<sub>2</sub>O<sub>3</sub>. There is a strong possibility of adverse chemical reactions between SiO<sub>2</sub> and liquid sodium. Physical properties of the material are reported in Table IV.

Table III. Chemical Analysis of Kaiser "Morex" Firebrick (ignited)

Oxide	Percent
CaO	0.60
Al <sub>2</sub> O <sub>3</sub>	37.80
SiO <sub>2</sub>	55.92
Fe <sub>2</sub> O <sub>3</sub>	1.95
MgO	0.62
TiO <sub>2</sub>	1.12
Alkalies	1.55

Table IV. Physical Properties of Kaiser "Morex" Firebrick

P. C. E. (Pyrometric Cone Equivalent) (ASTM: C 24)	32 - 33 (3135° F) (1724° C)
Hot Load Deformation - % (ASTM: C 16) 2460° F (1350° C)	0.5 - 2.0
Reheat (Linear Change - %) (ASTM: C 113) 5 Hr @ 2550° F (1400° C) 5 Hr @ 2732° F (1500° C)	-0.1 to +0.1 -0.1 to -0.7
Cold Crushing Strength, psi (ASTM: C 133) kgf/mm <sup>2</sup>	2300 - 3900 1.62 - 2.74
Modulus of Rupture, psi (ASTM: C 133) kgf/mm <sup>2</sup>	1150 - 1650 0.81 - 1.16
Panel Spalling (ASTM: C 107) High Duty - 2910° F (1600° C)	Under 10%
Bulk Density (lb/cu ft) (ASTM: C 20) (g/cm <sup>3</sup> )	133 - 137 2.13 - 2.19
Apparent Porosity - % (ASTM: C 20)	15 - 19
Apparent Specific Gravity (ASTM: C 20)	2.54 - 2.60

A representative of the manufacturer indicated that the melting point of the material was 3155° F (1737° C). In view of the nearly identical compositions of the insulating and fire-retardant brick, it is not clear why there should be as large a difference (405° F) in the reported melting points.

Interactions between Morex brick and molten UO<sub>2</sub> were also examined in an experimental study supported by The Aerospace Corporation.<sup>9</sup> When molten UO<sub>2</sub> was poured on the brick to simulate transient thermal shock, there was little sign of interaction. Very little gas or vapor release was observed during the transient segment of the experiment. After sustained heating for 30 min, with a molten UO<sub>2</sub> pool in contact with the brick for

9 min, approximately 1.4 cm of material were eroded in the region directly under the electric arc electrode. This erosion in this time period is considered to be significant and is substantially greater than the erosion observed when molten  $\text{UO}_2$  was heated on MgO brick.

The fire-resistant brick formed a eutectic mixture with molten  $\text{UO}_2$  at  $\sim 1650^\circ\text{C}$ . A single layer of this brick will provide only very limited protection for the concrete from molten  $\text{UO}_2$ .

#### B. FFTF INSULATING FIREBRICK

A layer of insulating firebrick will be employed between the fire-retardant firebrick and concrete at the Fast Flux Test Facility. The firebrick proposed for use is manufactured by the A. P. Green Refractories Division of the United States Gypsum Co. at Mexico, Missouri, and is identified as G-20 firebrick.

The brick is white and contains visible voids over a large fraction of its surface. The largest void visible in a cross section of the brick was elliptical with principal axis length of approximately 0.5 cm. An average porosity of 81.8% was measured in our laboratories with a range of 79.8 to 84.1%. This high porosity presumably makes the brick a relatively good insulator. The brick has a density of only 0.60 to 0.70  $\text{g/cm}^3$ .

The material is soft and brittle and an indentation can be easily made with a fingernail. When rubbed, a film came off the brick in a way similar to chalk.

An analysis of the brick was provided by the manufacturer. It is composed principally of  $\text{SiO}_2$  and  $\text{Al}_2\text{O}_3$  as indicated by the chemical analysis shown in Table V. The high  $\text{SiO}_2$  concentration may result in reactions between liquid sodium and this constituent.

The manufacturer's literature states that the brick can be used where the temperature does not exceed  $2000^\circ\text{F}$  ( $1093^\circ\text{C}$ ) and where slagging does not occur. A representative of the manufacturer indicated that it melts at approximately  $2750^\circ\text{F}$  ( $1510^\circ\text{C}$ ).



Table V. Chemical Analysis of A. P. Green  
G-20 Insulating Firebrick (ignited)

Oxide	Percent
SiO <sub>2</sub>	57 - 60
Al <sub>2</sub> O <sub>3</sub>	33 - 36
Fe <sub>2</sub> O <sub>3</sub>	1 - 2
CaO	0.1 - 1.6
MgO	0.01 - 0.6
TiO <sub>2</sub>	1.5 - 2.5
Alkalies	1 - 2

If this firebrick comes into contact with sodium during an accident, it may float to the top of the sodium pool. When a brick specimen was placed in water, it immediately absorbed water and sank to the bottom. It is not clear that the firebrick will behave in the same way in liquid sodium as a result of the higher surface tension of sodium. If sodium does not wet the brick or enter the pores, the brick will float to the surface unless it is restrained in some manner.

The interactions between molten UO<sub>2</sub> and this insulating brick were examined in experimental studies supported by The Aerospace Corporation.<sup>9</sup> When molten UO<sub>2</sub> was poured on the specimen to simulate thermal shock, the top 2 in. of the specimen melted. This represents substantial mass erosion even when the low density of the material is considered. The insulating firebrick provides essentially no protection against molten UO<sub>2</sub> because of its low density and melting point. Since only a 2.5-cm thick layer of material remained after the transient pouring phase, no attempt was made to proceed to the sustained heating part of the experiment. Very little gas evolution was observed during the course of the transient experiment. The evolving gases included small percentages of H<sub>2</sub>, CO, and CO<sub>2</sub>.

## VII. ANALYSIS OF SPECIMENS FROM EARLIER MOLTEN CORE DEBRIS - CONCRETE EXPERIMENTS AT THE AEROSPACE CORPORATION

During FY 77 a number of experiments were conducted at The Aerospace Corporation in which the interactions between molten  $\text{UO}_2$  and concrete were studied. In these experiments molten  $\text{UO}_2$  was first poured on a specimen under study to simulate thermal shock. After the specimen cooled, it was placed in another furnace and the  $\text{UO}_2$  was remelted to simulate long-term heating. Results from the analysis of specimens from these tests have become available during the current contract period and are discussed below. Other aspects of the experiments have been reported in detail in earlier reports.<sup>1, 2</sup>

### A. MOLTEN $\text{UO}_2$ -HEDL BASALT CONCRETE EXPERIMENTS

The material tested was cut from a test cylinder of basalt concrete prepared at HEDL. The cylinder was poured from material employed in the construction of FFTF.

Microscopic examination of polished cross sections of this concrete indicated that the aggregate was composed of gravels typical of riverine deposits with scoriated basalt as a major component. Many of the large and fine aggregates, however, appeared to be of granite origin. A large proportion of these are probably andesite, felsite, and small quartz grains.

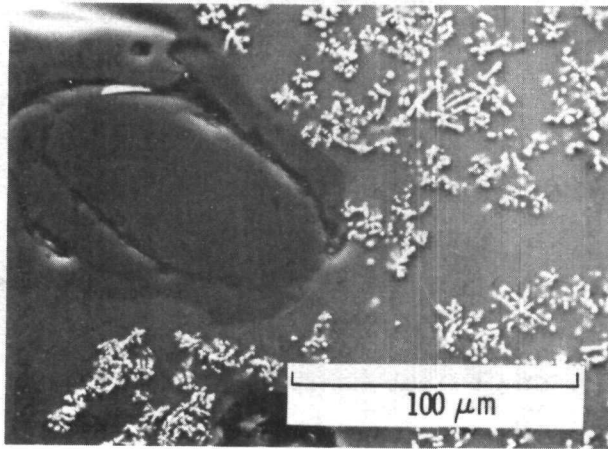
Several experiments in which concrete was melted were conducted in a muffle furnace and showed that different concrete aggregate particles melted at disparate temperatures and possessed differing viscosities in the molten state. For example, white felsite aggregate, a constituent of HEDL basalt concrete, melted at  $1095^\circ\text{C}$ ; the remainder of the aggregate melted into a very low viscosity pool at  $1250^\circ\text{C}$ . HEDL magnetite concrete, however, began to melt at  $1200^\circ\text{C}$  and became a very viscous liquid at  $1400^\circ\text{C}$ .

Differences in the viscosities of the various molten concrete aggregates should affect the rate at which they are mixed with molten uranium dioxide. Consequently, molten basalt concrete should be mixed with molten uranium dioxide more rapidly than molten magnetite concrete.

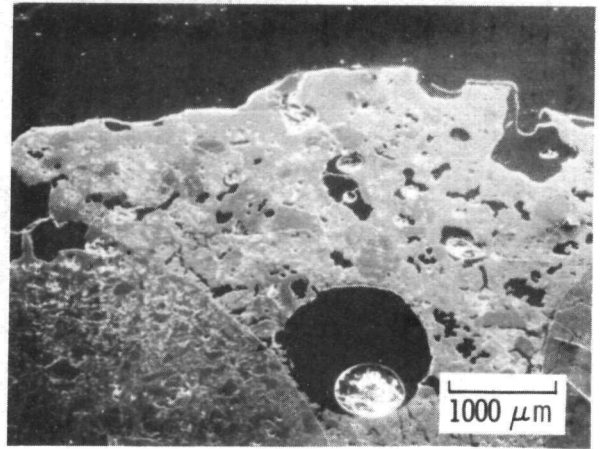
Varied rates of melting were also observed in tests where urania was sustained in a molten state for long periods of time while in contact with basalt, magnetite, and limestone concretes. Basalt concrete melted more rapidly than the magnetite and limestone concretes. The melted urania was maintained in a molten state for 24 min while in contact with basalt concrete. The molten basalt concrete dissolved into the molten urania forming what appeared to be a single liquid. After heating ended, the pool cooled to approximately 900°C where the mixture solidified and bubbling ceased.

Examination of a polished cross section of the melt in the scanning electron microscope (SEM) revealed a dendritic growth which was dispersed throughout the melt layer (Fig. 2a). The urania dendrites extending for a distance of approximately 800  $\mu\text{m}$  above the concrete interface were approximately 1/5 the size of those in the upper regions of the melt. The dendrites averaged 50  $\mu\text{m}$  across in the upper melt regions and 10  $\mu\text{m}$  across in the boundary zone. This difference in size can be attributed to a smaller concentration of uranium dioxide near the concrete-melt interface. The uranium dioxide dendrites crystallized out of the molten pool as a primary phase in the condensed system of  $\text{CaO-SiO}_2\text{-Fe}_2\text{O}_3\text{-UO}_2$ . Analysis confirmed that a single low viscosity liquid was formed when molten uranium dioxide and basalt concrete came in contact. Convective heat transfer effects should increase the potential for a greater rate of penetration into basalt concrete as compared to a higher viscosity mixture such as would be formed between  $\text{UO}_2$  and magnetite concrete.

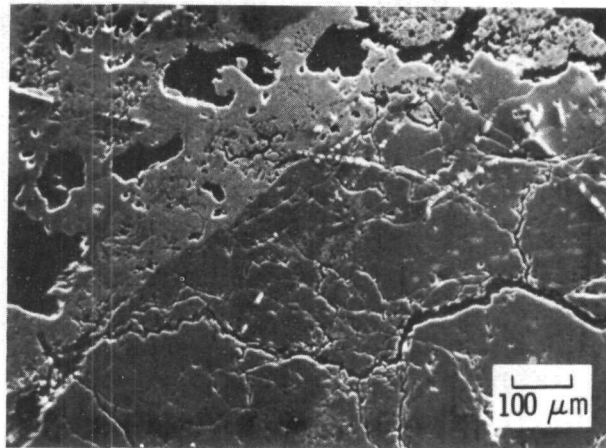
The large difference in temperature between the melting points of uranium dioxide and basalt concrete was sufficient to allow the crystallization of uranium dioxide from the basalt concrete melt. The very high rate of



(a)



(b)



(c)

Fig. 2. Molten  $\text{UO}_2$  - Basalt Concrete Experiment. (a) SEM photomicrograph of a quartz particle softening into a high viscosity liquid. The dark gray area is quartz and the light gray area is basalt concrete glass. The white particles are uranium dioxide crystals. (b) SEM cross section of solidified urania and basalt concrete melt in contact with basalt aggregate. The aggregate can be seen at the lower corners of the picture. The dark areas are gas pockets. Shrinkage cracks induced during cooling can be seen in the sintered cement phase between the two aggregate particles. EDAX examination showed urania in the upper melt layer above the aggregate particles. (c) SEM microphotograph of columnar basalt aggregate with microcracks in the surface in contact with the melt. The light gray areas at top are basalt concrete glass containing imbedded solidified  $\text{UO}_2$  particles. The dark gray area at the lower right is unmelted basalt aggregate.

cooling in our experiments prevented the occurrence of equilibrium conditions required for other crystallizations and phase changes. Analysis of the cubic crystals showed that they were essentially pure uranium dioxide. No layer formation resulting from differences in density between the molten  $\text{UO}_2$  and molten basalt concrete was observed. Layer formation was probably prevented by the rapid cooling rate and by substantial convection currents.

In Fig. 2a, a quartz particle is shown in the process of dissolving while in contact with the molten uranium dioxide - basalt concrete pool. The thick boundary visible around the quartz particle does not contain any of the components found throughout the remainder of the melt. Since quartz softens into a very viscous liquid, the absence of other constituents from the molten pool demonstrates the effect of high viscosity on the rate of solution of quartz into the molten pool.

Figure 2b is a lower magnification view of the melt and aggregate boundary. The dark area at the top of the picture is potting resin, which also fills gas pockets in the melting aggregate region. Two different mineral structures were visible in the basalt aggregate. The groundmass or matrix of the porphyric basalt (basalt containing dense, higher melting, particulate basalt crystals, or phenocrysts, suspended in a continuous phase of basalt), melted away at the aggregate-molten pool interface leaving phenocrysts (higher melting crystals) of harder basalt particles unmelted. Cracking of the cement region between the two fine aggregate particles, shown at the lower corners of the picture, is attributed to contraction of the specimen on cooling to room temperature. The higher melting columnar basalt aggregate contained fine microcracks penetrating approximately 500  $\mu\text{m}$  from the aggregate-melt interface (Fig. 2c). Examination of boundary zone (within the resolution of the coupled SEM-EDAX system) has shown that urania is present in the melted region but not in the unmelted aggregate or in the unmelted cement which fills the grain boundaries.

In summary, the molten layer above the basalt concrete consisted of a solidified homogeneous mixture with uranium dioxide crystals dispersed throughout. Uranium dioxide crystals which formed during cooling left the remaining components in a solution that solidified as a glass at a lower temperature. Uranium dioxide was the primary phase of the mixture. Rapid cooling resulted in nonequilibrium conditions which prevented further phase separations. Variations in the composition of the basalt aggregate caused melting of basalt concrete by molten uranium dioxide to vary because of differences in viscosity and solubility.

Large cracks were formed in the cement paste and fine aggregate matrix, between the large aggregate, by the decomposition of the hydrated cement and sintering together of fine particles at the high temperatures. This weakened the concrete and allowed the molten uranium dioxide to rapidly melt the low density fine basalt particles.

The low melting points of many of the aggregates and the low viscosity of melted basalt allowed a more rapid progress by the molten pool into basalt concrete as compared with the other types of concrete.

#### B. MOLTEN UO<sub>2</sub>-MAGNETITE CONCRETE EXPERIMENTS

Microscopic examination of magnetite aggregate revealed many needle-like structures imbedded in much of the aggregate. SEM-EDAX analysis showed that the needles had a high titanium content. The quantitative chemical analysis also indicated a significant titanium content in the aggregate. The aggregate is actually titaniferrous magnetite.

Laboratory tests of magnetite concrete in a muffle furnace showed that melting of the cement and fine aggregate phase occurred before melting of the coarse magnetite aggregate. Complete melting of magnetite concrete occurred at approximately 1400°C to 1530°C, forming a very viscous liquid. The high viscosity of molten concrete inhibited rapid diffusion into the molten uranium dioxide and slowed convective circulation of the fine

unmelted concrete particles into the molten uranium dioxide. No layering due to differences in density of the two components of the molten pool was observed.

Examination of a polished cross section of the solidified uranium dioxide-magnetite concrete indicated that molten uranium dioxide and molten magnetite concrete existed as two immiscible liquids. Evidence of immiscibility can be seen in Fig. 3, where the molten uranium dioxide solidified at high temperatures in globules dispersed throughout the melt. The high iron content crystals are thought to have solidified at a lower temperature than the globules of uranium dioxide. It is known that the magnetite crystal structure is cubic, forming an octahedral or dodecahedral structure. Hematite, a higher oxide of iron, has a rhombohedral crystal structure and cross sections of the rhombohedra often have a hexagonal shape. Hexagonal crystals can be seen in Fig. 3. EDAX maps of the area, shown in the photograph, indicate that the globules contain only uranium and the hexagonal crystals contain only iron. Calcium and silicon were found in the interstices between the hexagonal crystals forming a low temperature glassy phase.

The conversion of melted magnetite (a mixed  $\text{Fe}^{+2} - \text{Fe}^{+3}$  oxide) to hematite ( $\text{Fe}_2\text{O}_3$ ) can be accounted for by oxidation by the 2% oxygen atmosphere present above the melt.

In summary, the molten layer above the magnetite concrete was composed of molten uranium dioxide and molten magnetite concrete existing as two immiscible liquids with no evidence of layer formation resulting from density differences. The uranium dioxide solidified into globules, without crystal growth, indicating that it was not in solution in the molten pool. The molten magnetite is thought to have dissolved in the molten concrete liquid phase, crystallizing out as hematite. The calcia and silica remained as a glass on cooling to room temperature.

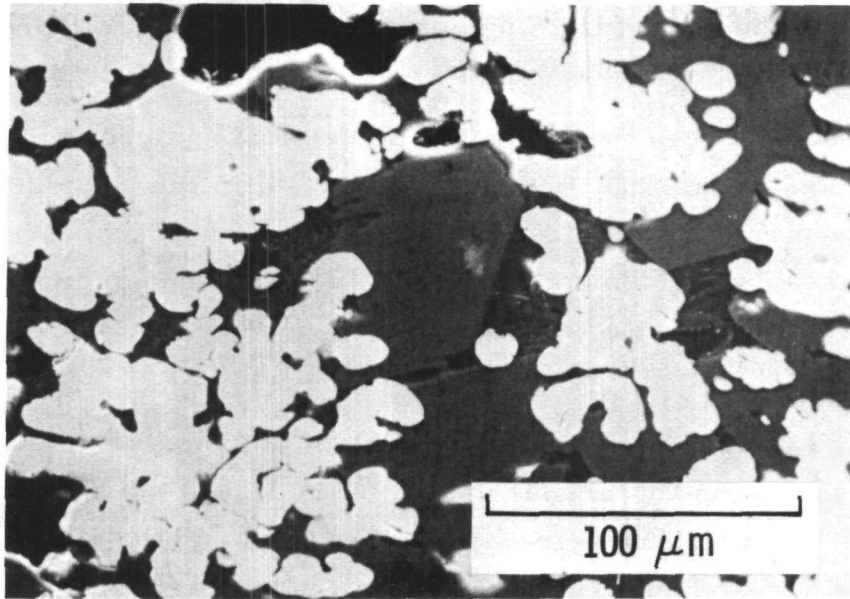


Fig. 3. SEM Photomicrograph of Solidified Molten Uranium Dioxide and Magnetite Concrete. The white areas are uranium dioxide globules and the light gray hexagonal structures are hematite crystals. The dark gray areas are a calcia-silica glassy phase.



### C. MOLTEN UO<sub>2</sub>-LIMESTONE CONCRETE INTERACTIONS

Relative penetration rates of molten UO<sub>2</sub> into several concretes were reported in our June 1977 Annual Report.<sup>1</sup> The concretes included two different limestone concrete formulations proposed for use in the Clinch River Breeder Reactor. The original formulation is designated Tennessee limestone concrete and the revised formulation is designated CRBRP limestone concrete.

A comparison between the quantitative chemical analyses of the two limestone concretes shows that there is very little difference chemically between the two concretes as indicated in Table VI. The Tennessee limestone concrete uses Type I cement and 1-1/2-in. limestone aggregate while the CRBRP limestone concrete uses modified Type II cement and 3/4-in. aggregate.

Examination of optical photomicrographs of polished cross sections of the concrete shows the calcareous nature of the limestone aggregates. Figure 4a shows two differing aggregates, one containing the round relic structures of zooplankton and the other having random wavy structures left from algae growths. The fine limestone aggregate and cement phase fills the area between the two large aggregate particles.

Thermal decomposition of limestone concrete by molten UO<sub>2</sub> will convert water of hydration to steam when heated above 100°C. Decomposition of the carbonates in the fine and coarse aggregate will also produce large quantities of carbon dioxide when the temperature of the limestone concrete reaches 950°C. These gases will vent rapidly through the friable decomposed concrete and the UO<sub>2</sub>-limestone concrete interface, and will percolate through the molten UO<sub>2</sub> melt. It has been suggested that a gas layer will form at the concrete-molten UO<sub>2</sub> interface and significantly influence the heat flow into the concrete.

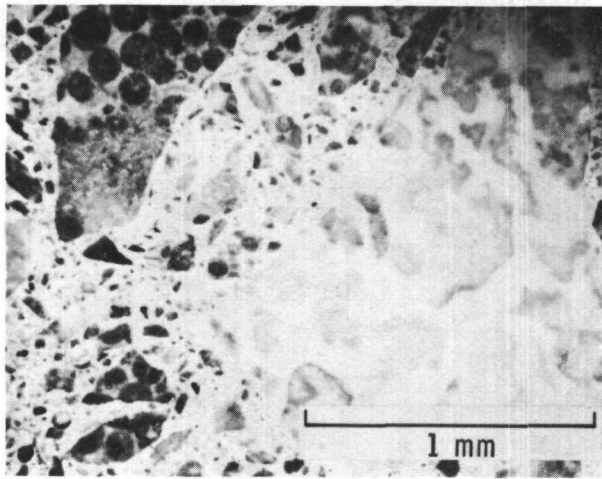
Table VI. Percentage of Component Oxides in Two Limestone Concretes

Oxide	Tennessee Limestone Concrete	CRBRP Concrete
CaO	52.9	50.7
SiO <sub>2</sub>	4.4	5.1
Fe <sub>2</sub> O <sub>3</sub>	1.4	1.0
Al <sub>2</sub> O <sub>3</sub>	1.3	2.2
MgO	1.7	2.9
Na <sub>2</sub> O	0.1	0.1
H <sub>2</sub> O	2.2	1.7
SO <sub>3</sub>	0.4	0.5
Ignition loss	38.8	38.6

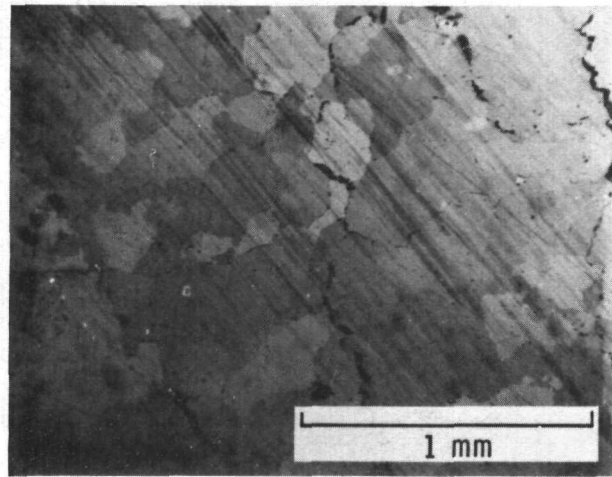
In the CRBRP limestone concrete sustained heating experiment, the concrete was eroded to a depth of 1.4 cm after 35 min of heating. Our analyses showed that only uranium oxides were present in the upper 0.5 cm of the solidified melt. Optical and SEM photomicrographs show the crystallization that took place on cooling. Adjacent crystals can be seen with differing orientations in polarized light (Fig. 4b).

In the region 0.5 cm below the upper surface of the melt, dendrites grew from the solidified UO<sub>2</sub> into numerous voids found in this region. This is shown in Fig. 4c.

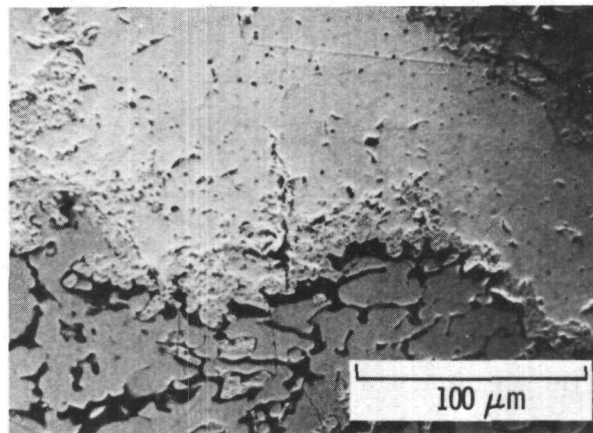
The solidified uranium dioxide particles and dendrites are surrounded by a layer of porous material with a very fine structure from 10- to 30- $\mu$ m thick. SEM-EDAX analyses indicated that the uranium concentration in this



(a)



(b)



(c)

Fig. 4. Molten  $\text{UO}_2$  - Limestone Concrete Experiment. (a) Optical photomicrograph of small limestone aggregate particles in a matrix of finer limestone aggregate and cement. Round relic structures of zooplankton are visible in the aggregate at the upper left. Wavy structures in the aggregate particle at the right are relic algae deposits found in limestone. (b) Optical photomicrograph of solidified  $\text{UO}_2$  under polarized light.  $\text{UO}_2$  crystals of differing orientations are visible as different shades of gray. The larger cracks are filled with impurities. (c) SEM photomicrograph of solidified  $\text{UO}_2$  surrounded by a  $\text{CaO-UO}_2$  eutectic phase. The light gray area is solidified  $\text{UO}_2$  and the dark gray area is a  $\text{CaO-SiO}_2\text{-UO}_2$  glass phase. Black areas are voids.

layer was higher than in the glassy phase found in the regions between and below the dendrites.  $\text{UO}_2$ ,  $\text{CaO}$ , and  $\text{SiO}_2$  were all found in the glass phase. The concentrations of calcium in the porous layer adjacent to the solidified  $\text{UO}_2$  and in the glass were approximately equal, but silicon was only found in the glassy phase. The phase diagram of the  $\text{CaO-UO}_2$  system indicates the presence of a eutectic phase corresponding to 45 wt%  $\text{CaO}$  in  $\text{UO}_2$  with a freezing point of  $2080^\circ\text{C}$ .

In summary, molten  $\text{UO}_2$  in contact with limestone concrete caused dehydration of the concrete and dissociation of the magnesium and calcium carbonates in the aggregate, releasing large quantities of steam and carbon dioxide gas. It is thought that the cement phase (as opposed to the aggregate) melted first at the original cement clinker\* temperature, forming a glass which at higher temperatures reacted with calcia from the aggregate. Above the  $\text{CaO-UO}_2$  eutectic temperature of  $2080^\circ\text{C}$ ,  $\text{UO}_2$  was incorporated in the molten mixture. On cooldown,  $\text{UO}_2$  crystallized out of the melt and a  $\text{CaO-UO}_2$  eutectic boundary layer formed around the solidified  $\text{UO}_2$ . A  $\text{CaO-SiO}_2\text{-UO}_2$  glass solidified at lower temperatures.

D. TYPE 304 MOLTEN STAINLESS STEEL-CRBRP TYPE  
LIMESTONE CONCRETE EXPERIMENTS

The limestone concrete was made to CRBRP specification in our laboratory from aggregate, sand, and cement obtained from the reactor site area. Molten 304 stainless steel was arc melted in a tilt-pour furnace and poured on the concrete specimen to simulate thermal shock from a hypothetical core meltdown accident in the Clinch River Breeder Reactor. After the specimen cooled, it was placed in another arc furnace and the stainless steel was remelted for 23 min.

---

\*The clinker is a product of firing naturally occurring clays and limestone into a partly fused mass for later grinding into Portland cement.

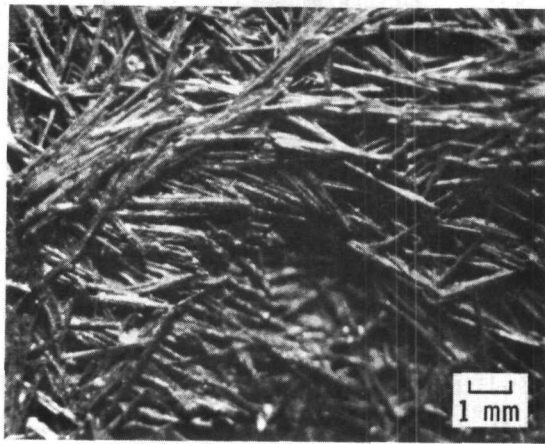
Vigorous bubbling of gas through the molten stainless steel occurred during the melt cycle and continued for a half-minute after power was terminated, until the metal solidified. A brown slag formed on the top of the molten metal and remained there during the experiment. The liquid metal and molten slag appeared to be immiscible.

On removal from the specimen holder, it was found that the solidified metal did not adhere to the concrete. When the casting was visually examined, it was found that the lower face, in contact with the concrete, was covered with a matted layer of very stiff fibers as shown in Fig. 5a. The upper surface also had a matted fibrous appearance.

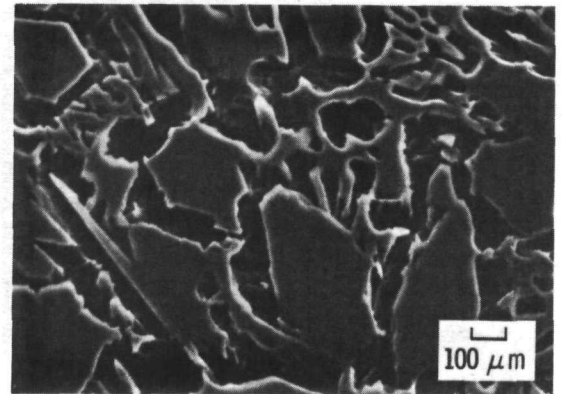
Cross sectioning of the solidified metal casting for microscopic analysis revealed acicular structures throughout the whole specimen. Many voids were present which were attributed to gas bubbling through the molten metal during the melting period of the experiment. Many of the hexagonal needles have a small  $1.5 \mu\text{m}$  hole running down the axis of the needle, Fig. 5b. The widths of the needles at the bottom of the steel casting averaged  $20 \mu\text{m}$  across parallel surfaces. At the top of the steel casting the needles average 5 to  $10 \mu\text{m}$  across. The average length of the needles was  $200 \mu\text{m}$ .

The average microhardness of the cross-sectional surface of the needles was 58 on the Rockwell b scale. Hairline cracks from the diamond shaped indentations propagated to the needle-matrix interface indicating that the measured hardness value is much lower than the actual hardness value. The average microhardness of the matrix was 22 on the Rockwell c scale with a minimum value of 98 on the Rockwell b scale. The average microhardness of the stainless steel starting material was 84 on the Rockwell b scale. Thus, the needles were not as hard as the starting material, which in turn was less hard than the matrix.

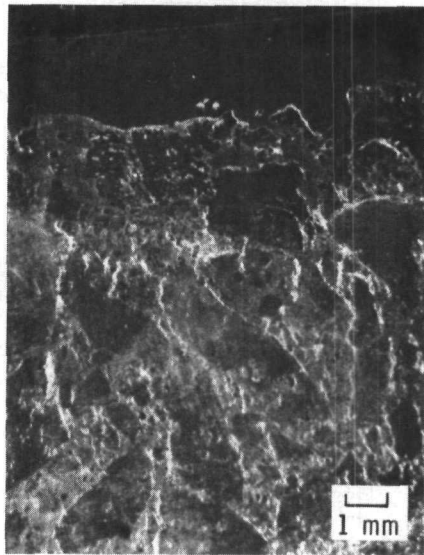
EDAX examination of the needles indicated that the needles were richer in chromium than the matrix but weaker in iron and nickel.



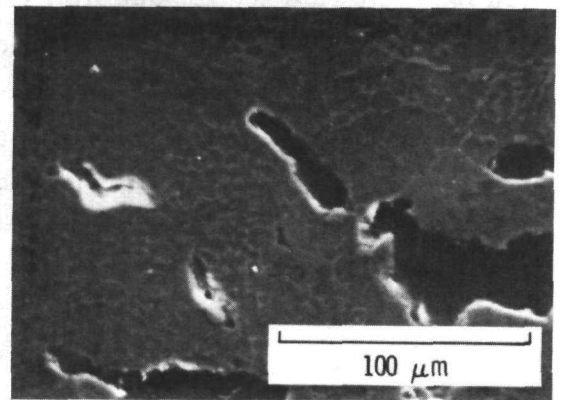
(a)



(b)



(c)



(d)

Fig. 5. Molten Stainless Steel - Limestone Concrete Experiment. (a) SEM view of lower face of a solidified stainless steel casting showing the acicular structure of the metallic surface. The specimen was in contact with limestone concrete during the experiment. (b) SEM photograph of the cross section of hexagonal needles observed throughout the solidified stainless steel. Note the small hole visible in many of the needles. (c) SEM cross section of limestone concrete-stainless steel interface after removal of stainless steel. A thin layer of melted concrete was observed adhering to the unmelted concrete. Most of the molten concrete rose through the molten steel appearing at the top as a layer of slag. The solidified steel separated from the concrete without adhesion. The dark area at the top is potting resin and a porous melt layer and darker fired aggregate particles are visible above the light gray concrete aggregate. (d) Cross section of melted concrete layer adhering to limestone concrete. The dark areas are voids and the light gray areas are concrete. The dark gray area is steel showing immiscibility with molten concrete.

Although most of the molten concrete floated up through the molten stainless steel, a small layer of molten concrete was found at the top surface of the concrete. This layer averaged 1.5 mm in thickness as shown in Fig. 5c. Molten steel was present in this molten concrete layer but was immiscible with the concrete. EDAX examination of this molten layer showed that calcia, silica, and iron were present in large amounts (Fig. 5d).

Our analysis indicates that the molten stainless steel heats the limestone concrete causing the release of water vapor. Dissociation of calcium carbonate in the heated limestone aggregate and cement paste released carbon dioxide which bubbled vigorously through the molten steel. The molten steel is visible in the molten concrete layer that adhered to the unconverted concrete. However, EDAX examination showed that the steel did not penetrate beyond this layer. The acicular structure, thought to be a chromium-rich carbide generated in the stainless steel, apparently resulted from the bubbling of  $\text{CO}_2$  through the melt.

## REFERENCES

1. D. G. Swanson, D. M. Goddard, E. H. Zehms, J. D. McClelland, R. A. Meyer, H. L. L. van Paassen, and G. D. Kidwell, Annual Progress Report - Evaluation of Materials for CRBRP Core Retention, ATR-77(7608)-2, The Aerospace Corporation (June 1977).
2. D. G. Swanson, E. H. Zehms, C. Y. Ang, J. D. McClelland, R. A. Meyer, and H. L. L. van Paassen, Annual Progress Report - Ex-Vessel Core Catcher Materials Interactions, ATR-77(7608)-1, The Aerospace Corporation (October 1976).
3. J. A. Hassberger, et al., Hanford Engineering Development Laboratory, private communications.
4. R. L. Coats, et al., Sandia Laboratories, private communications.
5. S. A. Meacham, Molten Stainless Steel and Urania Compatibility with Refractory Materials Considered for CRBRP Parallel Design Ex-Vessel Core Retainers, Westinghouse Advanced Reactors Division, CRBRP-ARD-0098.
6. R. P. Stein, L. Baker, Jr., W. H. Gunther, and C. Cook, Interaction of Heat Generating Molten  $UO_2$  with Structural Materials, Argonne National Laboratory, ANL-78-10.
7. D. A. Powers, Sandia Laboratories, private communication.
8. D. A. Powers, D. A. Dahlgren, J. F. Muir, and W. D. Murfin, Exploratory Study of Molten Core Material/Concrete Interactions, Sandia Laboratories, SAND 77-2042.
9. D. G. Swanson, H. L. L. van Paassen, and A.R. Marchese, The Aerospace Corporation, to be published.



<b>NRC FORM 335</b> (7-77)		<b>U.S. NUCLEAR REGULATORY COMMISSION</b> <b>BIBLIOGRAPHIC DATA SHEET</b>		1. REPORT NUMBER <i>(Assigned by DDC)</i> NUREG/CR-0900	
4. TITLE AND SUBTITLE <i>(Add Volume No., if appropriate)</i> Annual Progress Report Evaluation of Materials for Retention of Sodium and Core Debris in Reactor Systems				2. <i>(Leave blank)</i>	
7. AUTHOR(S) D. G. Swanson, E. H. Zehms, R. A. Meyer, J. S. McClelland, and H. L. L. van Paassen				3. RECIPIENT'S ACCESSION NO.	
9. PERFORMING ORGANIZATION NAME AND MAILING ADDRESS <i>(Include Zip Code)</i> Aerospace Corporation Materials Sciences Laboratory P. O. Box 92957 Los Angeles, California 90009				5. DATE REPORT COMPLETED MONTH June YEAR 1979	
12. SPONSORING ORGANIZATION NAME AND MAILING ADDRESS <i>(Include Zip Code)</i> U. S. Nuclear Regulatory Commission Office of Nuclear Reactor Regulation Washington, D. C. 20555				DATE REPORT ISSUED MONTH YEAR	
13. TYPE OF REPORT Technical				6. <i>(Leave blank)</i>	
15. SUPPLEMENTARY NOTES				8. <i>(Leave blank)</i>	
16. ABSTRACT <i>(200 words or less)</i>  This report considers some of the consequences of a hypothetical core disruptive accident in a nuclear reactor. The interactions expected between molten core debris, liquid sodium, and materials that might be employed in an ex-vessel sacrificial-bed or in the reactor building are discussed. Experimental work performed for NRC by Sandia Laboratories and Hanford Engineering Development Laboratory on the interactions between liquid sodium and basalt concrete is reviewed. Studies of molten steel interactions with concrete at Sandia Laboratories and molten UO <sub>2</sub> interactions with concrete at The Aerospace Corporation are also discussed. The potential of MgO for use in core containment is discussed and refractory materials other than MgO are reviewed. Finally, results from earlier experiments with molten core debris and various materials performed at The Aerospace Corporation are presented.				10. PROJECT/TASK/WORK UNIT NO.	
17. KEY WORDS AND DOCUMENT ANALYSIS				11. CONTRACT NO. NRC-03-79-126	
17b. IDENTIFIERS/OPEN-ENDED TERMS				13. TYPE OF REPORT Technical	
18. AVAILABILITY STATEMENT No Restrictions on Availability				PERIOD COVERED <i>(Inclusive dates)</i> September 30, 1977-December 30, 1978	
19. SECURITY CLASS <i>(This report)</i> Unclassified				14. <i>(Leave blank)</i>	
20. SECURITY CLASS <i>(This page)</i> Unclassified				21. NO. OF PAGES	
22. PRICE \$				22. PRICE \$	